Proceedings of the Korean Nuclear Society Autumn Meeting
Taejon, Korea, October 2000

Analysis of Direct Vessel Injection Impingement Flow

Sang Hyuk Yoon, Yun-Kang Park, Kune Y. Suh
Chul Hwa Song*, Moon Ki Chung*, Jong-Kyun Park*

Department of Nuclear Engineering, Seoul National University
San 56-1 Shinrim-dong, Kwanak-gu, Seoul, 151-742, Korea
Phone : +82-2-880-8281, Fax : +82-2-883-0827, Email : mrysh@plaza1.snu.ac.kr
*Korea Atomic Energy Research Institute
P.O. Box 105, Yusong, Taejon, 305-600, Korea

Abstract

The direct vessel injection (DVI) into the downcomer is one of the major design features of the Korean Next Generation Reactor (KNGR) emergency core cooling system (ECCS). For this type of the ECCS, however, the flow pattern in the downcomer during a loss-of-coolant accident (LOCA) has not yet been fully investigated. Also, the experimental and analytical studies on the hydraulic phenomena are not complete enough to allow for detailed design of the system. One of the important phenomena is the impingement by the ECC injection flow. To investigate the behavior of flow such as the impingement, it was necessary to first understand the injected flow motion on a vertical flat wall with well-defined boundary conditions. The experiment was conducted using two flat acryl plates. In this experiment, we measured the flow width by the conductance method as well as visual inspection. Results of the measurements are easily understandable. The flow width increases downstream. As the injection velocity increases, so does the flow width. The outer boundary of the fluid flow is thick. Also, the greater the injection velocity, the larger the flow width and the smaller the average film thickness. In an effort to understand the impingement flow characteristics observed from the tests, a simple numerical code was written to determine the width of flow on the flat plate. In reactor applications, flows from the four DVI lines may get in touch with one another, and thicken to interfere with upcoming steam to the extent the flooding characteristics and subsequently the amount of bypass flow in the downcomer may change. Experimental and numerical results shed light on the width of the DVI film flow, which is pivotal in determining the amount of ECC bypass due to flooding

1. INTRODUCTION

One of the salient features in the Korean Next Generation Reactor (KNGR) design is the direct vessel injection (DVI) system as demonstrated in Fig. 1. For this emergency core cooling system (ECCS), however, the flow pattern in the downcomer during a loss of coolant accident (LOCA) has not yet been fully investigated (Suh et al., 1998). Also, the experimental and analytical studies on the hydraulic behavior are not complete enough to allow for detailed design. If the behavior of the injected flow in the downcomer during a LOCA is predicted correctly, the reflood capability of the DVI system should be acceptable to protect against the core uncovery. One of the unknown characteristics is the flow velocity profile. One can obtain the information in an analytical,

numerical, or experimental way. First, the analytical method turns out to be limited in solving the problem at hand because many unknown phenomenological parameters persist. The mathematical and physical solution methods do not necessarily yield the correct flow pattern, either. To investigate the behavior of flow, it was necessary to understand the injected flow motion on a vertical flat wall. Two flat acryl plates were used for the experiment. The conductance method aided by visual inspection was used to measure the flow width. The average vertical velocity was then calculated approximately using the continuity equation. Results of the measurements are easily understandable.

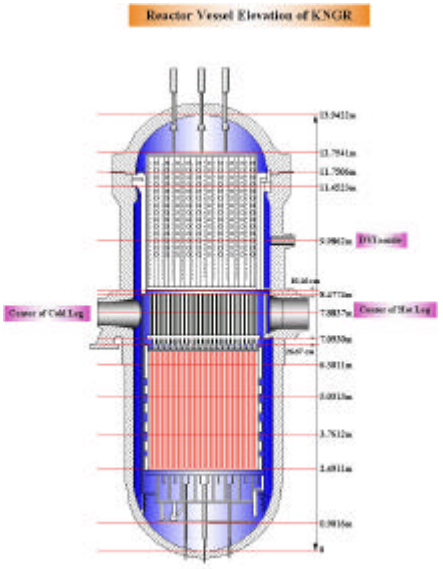

Fig. 1 DVI system geometry for KNGR

The flow width increases downstream. As the injection velocity increases, so does the flow width. The outer boundary of the fluid flow is thick. Also, the greater the injection velocity, the larger the flow width and the smaller the average film thickness. In an effort to understand the impingement flow characteristics observed from the tests, the potential function and the Navier-Stokes equations are numerically solved for the impingement region and the wall jet region, respectively. Experimental and numerical results shed light on the width of the DVI film flow.

2. NUMERICAL ANALYSIS

Two basic differential equations are used in this study, i.e. the continuity and momentum equations for the fluid motion. At the nozzle exit, the velocity is assumed to be of a fully developed flat profile. The nozzle has infinite length and zero thickness. The flow pattern depends on the injection velocity and the diameter of the injection nozzle. We assume that the fluid is incompressible and Newtonian. Figure 2 diagrammatically shows the flow configuration in the vicinity of the nozzle. The wall jet region is treated by the Navier-Stokes equations, while the impingement region is taken care of by the potential function for the stagnation point.

2.1 Impingement region

Coleman and Richard (1971) investigated the boundary between the impingement region and the wall jet region.

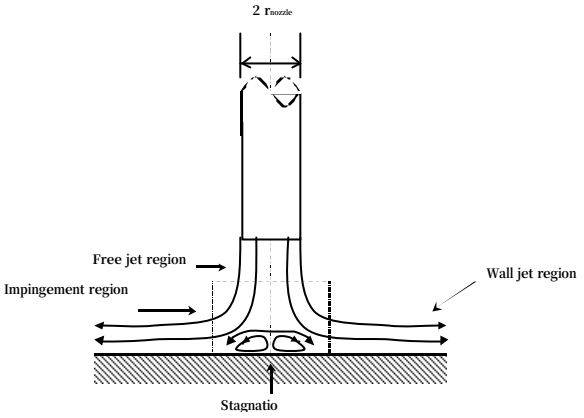

Fig. 2 Flow configuration

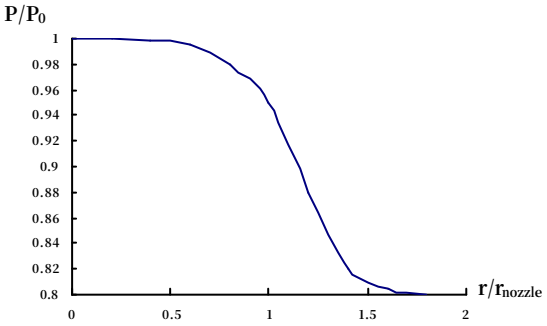

P_0 : the pressure at the stagnation point

Fig. 3 Stagnation region pressure distributions for flat surface (Mohan and Ramesh, 1982)

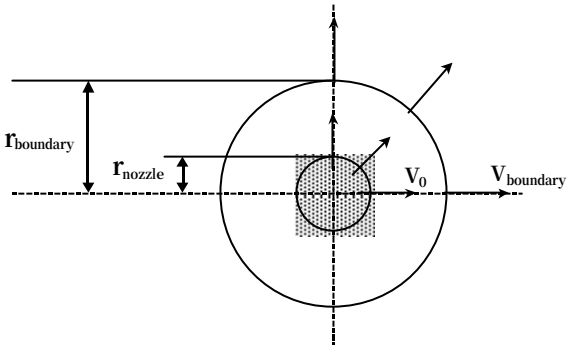

Fig. 4 Impingement region, plan view

Their results yielded the pressure distribution on the flat plate around the stagnation point. As shown in Fig. 3, the radius of the impingement region is about 1.8 times that of the nozzle.

$$r_{boundary} = 1.8 \times r_{radius} \tag{1}$$

The potential function of the impingement region is well described by a logarithmic function just like a line source in two dimensions. The gravity effect is ignored in the impingement region because the velocity of the impingement region is very high while the cross-sectional area of the flow is small. Thus the square of velocity is proportional to the potential logarithmic function.

$$V_{boundary} = \sqrt{\log r_{boundary} / \log r_{nozzle}} \times V_0 \tag{2}$$

The impingement region is depicted in Fig. 4 as seen from above.

2.2 Wall jet region

The gravitation and the friction are the important factors in the wall jet region as shown in Fig. 5 (White, 1994). Thus the momentum equation may be written as

$$\rho\frac{d\mathbf{V}}{dt} = -\nabla p + \rho\mathbf{g} + \mathbf{F}_{friction} \tag{3a}$$

Since the pressure-gradient factor is zero in the wall jet region, Equation (3a) may be simplified as follows

$$\rho\frac{d\mathbf{V}}{dt} = \rho\mathbf{g} + \mathbf{F}_{friction} \tag{3b}$$

If the fluid is incompressible, the continuity indicates that the volume flow is constant. Thus

$$V \propto \frac{1}{z}$$

Therefore,

$$F_{friction} = \mu\frac{dV}{dz} \propto \mu(dV)^2 \tag{4}$$

In the rectangular coordinate system, Equations (3b) and (4) yield the following expressions:

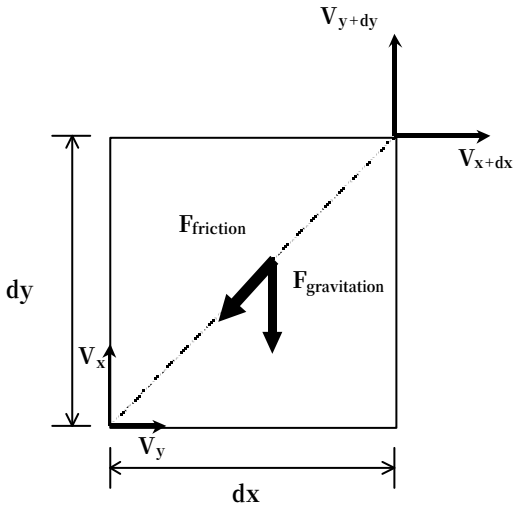

Fig. 5 Infinitesimal area in the wall jet region

$$a_x = a\cos\theta = \frac{dV_x}{dt} = -\frac{\mu}{\rho}(dV_{av})^2 \cos\theta \tag{5a}$$

$$a_y = a\sin\theta = \frac{dV_y}{dt} = \mu\frac{\mu}{\rho}(dV_{av})^2 \sin\theta - g \tag{5b}$$

where

$$dV_{av} = \sqrt{\left(\frac{V_x + V_{x+dx}}{2}\right)^2 + \left(\frac{V_y + V_{y+dy}}{2}\right)^2}$$

The minus sign is for downward flow, and the plus sign is for upward flow, respectively, in Equation (5b).

2.3 Computation

Equations (5a) and (5b) must be modified for numerical calculation as presented in Table 1.

Table 1. Modifications for computation

From	To	From	To
V_x	$V_{x(n)}$	V_y	$V_{y(n)}$
V_{x+dx}	$V_{x(n+1)}$	V_{y+dy}	$V_{y(n+1)}$

After all, Equation (5a) reduces to

$$\frac{V_{x(n+1)} - V_{x(n)}}{dt} = -\frac{m}{r}\left[\left(\frac{V_{x(n+1)} + V_{x(n)}}{2}\right)^2 + \left(\frac{V_{y(n+1)} + V_{y(n)}}{2}\right)^2\right]\frac{dx}{\sqrt{dx^2 + dy^2}}$$

or

$$\frac{V_{x(n+1)} - V_{x(n)}}{dt} = -\frac{m}{r}\left[\left(\frac{V_{x(n+1)} + V_{x(n)}}{2}\right)^2 + \left(\frac{V_{y(n+1)} + V_{y(n)}}{2}\right)^2\right]\frac{dx/dt}{\sqrt{\left(dx/dt\right)^2 + \left(dy/dt\right)^2}}$$

If the time interval, dt, is very short, following approximations may be made:

$$\frac{V_{x(n+1)} + V_{x(n)}}{2} \approx V_{x(n)} \quad , \quad \frac{V_{y(n+1)} + V_{y(n)}}{2} \approx V_{y(n)}$$

The above equations may be rewritten as

$$\frac{V_{x(n+1)} - V_{x(n)}}{dt} = -\frac{\mu}{\rho}\left[V_{x(n)}{}^2 + V_{y(n)}{}^2\right]\frac{V_{x(n)}}{\sqrt{V_{x(n)}^2 + V_{y(n)}^2}}$$

$$\frac{V_{x(n+1)} - V_{x(n)}}{dt} = -\frac{\mu}{\rho}\sqrt{V_{x(n)}^2 + V_{y(n)}^2}\cdot V_{x(n)}$$

$$V_{x(n+1)} = \left[-\frac{\mu}{\rho} \sqrt{V_{x(n)}^2 + V_{y(n)}^2} \cdot V_{x(n)} \right] dt + V_{x(n)} \tag{6a}$$

Equation (5b) may be transformed using the modifications in Table 1 as

$$\frac{V_{y(n+1)} - V_{y(n)}}{dt} = \mu \frac{\mu}{\rho} \sqrt{V_{x(n)}^2 + V_{y(n)}^2} \cdot V_{y(n)} - g$$

$$V_{y(n+1)} = \mu \frac{\mu}{\rho} \sqrt{V_{x(n)}^2 + V_{y(n)}^2} \cdot V_{y(n)} dt - g dt + V_{y(n)} \tag{6b}$$

Values for $V_{x(0)}$ and $V_{y(0)}$ are obtained by analysis in the impingement region. The flow pattern on the flat plate can be drawn through summation of $V_{x(n)}dt$ and $V_{y(n)}dt$ as

$$X = \sum V_{x(n)} dt$$

$$Y = \sum V_{y(n)} dt$$

3. RESULTS

3.1 Measurement data

Experiments were conducted utilizing the injection pipe of radius of 1.25cm, and the flow velocity of 42cm/s, 83cm/s and 124cm/s, respectively in the test apparatus shown in Fig. 6.

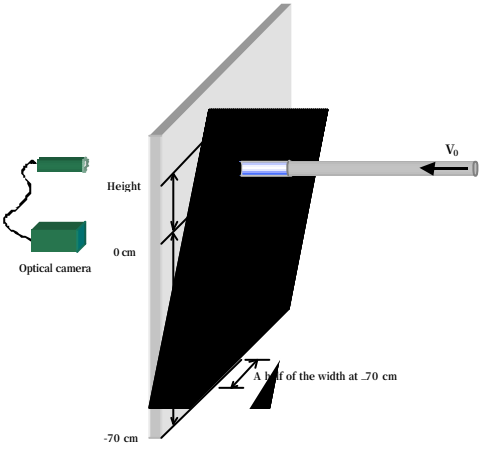

Fig. 6 The experiment setup

A transparent plate is utilized to facilitate identification of the shape of the flow. Figure 7 presents the results for the flow boundary. The center of the nozzle is located at the origin. The test results are summarized in Table 2.

Table 2. Results of the experiment

Injection Velocity	42 cm/s	83 cm/s	124 cm/s
Height	5.2 cm	13.4 cm	19.1 cm
Half Width at –70 cm	30.7 cm	42.4 cm	~50.0 cm

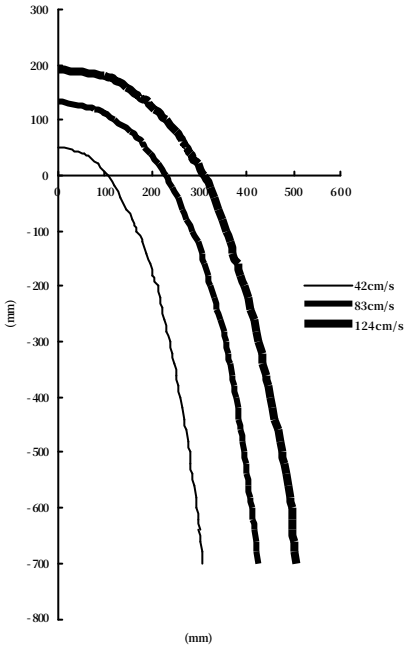

Fig. 7 Flow width data from the experiments

3.2 Computational results

Figures 8, 9, and 10 illustrate the results of the calculation for the expected flow pattern given the respective water injection velocities. Typical calculated results are collected in Table 3 for the height and a half of the flow film width at 70 cm below the point of water injection.

4. DISCUSSION

The deviation of the computed results from the measurement data is presented in Table 4. At the velocity of 83cm/s, the difference between the two results is minimal, while it is a bit large in other cases. One critical reason is that the experimental equipment was rather structurally unstable against fluctuations. The impact of the injection caused the error when the thickness of the flat plate was 1cm. But for the fluctuations observed during the tests, the difference may be decreased between the experimental and predictive results.

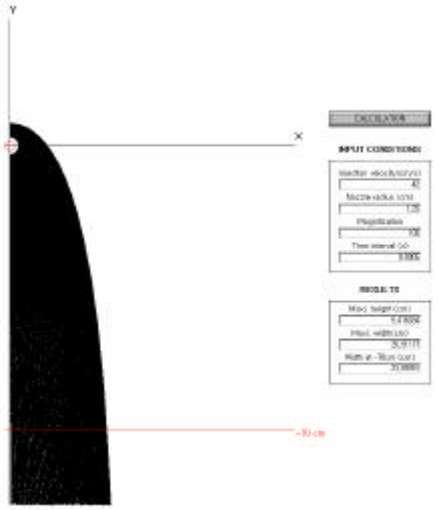

Fig. 8 Flow pattern at v = 42 cm/s

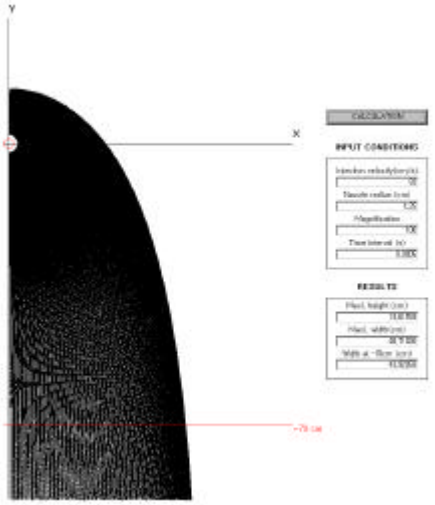

Fig. 9 Flow pattern at v = 83 cm/s

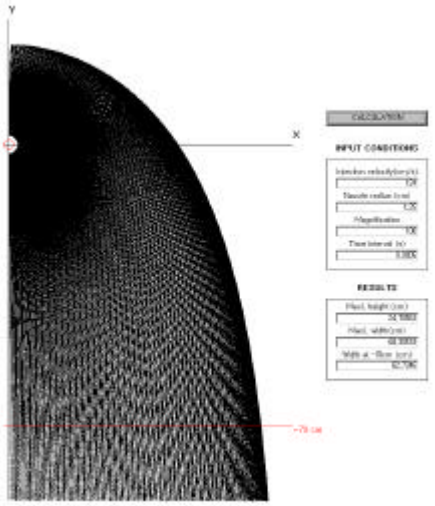

Fig. 10 Flow pattern at v = 124 cm/s

Table 3. Results of the computation

Injection Velocity	42 cm/s	83 cm/s	124 cm/s
Height	5.41 cm	13.61 cm	24.78 cm
Half Width at –70 cm	23.89 cm	43.92 cm	62.73 cm
Half Width (Maximum)	26.91 cm	48.71 cm	68.30 cm

Table 4. Difference between measured and computed values

Injection Velocity	42 cm/s	83 cm/s	124 cm/s
Height	3.8%	1.5%	22.9%
Half Width at –70 cm	22.1%	3.4%	26.7%

Now, we may investigate the DVI system that has the diameter of 21.59 cm (see Fig.1) using the numerical program. The boundary conditions were determined by TRAC (1984) during a large-break LOCA. According to TRAC, water from the DVI nozzle is injected at 16 sec after the LOCA and the velocity is about 23.53 m/s maximum. We predicted the flow pattern under the same condition as in the KNGR DVI system using the computational program. The values in Fig.11 are summarized in Table 5.

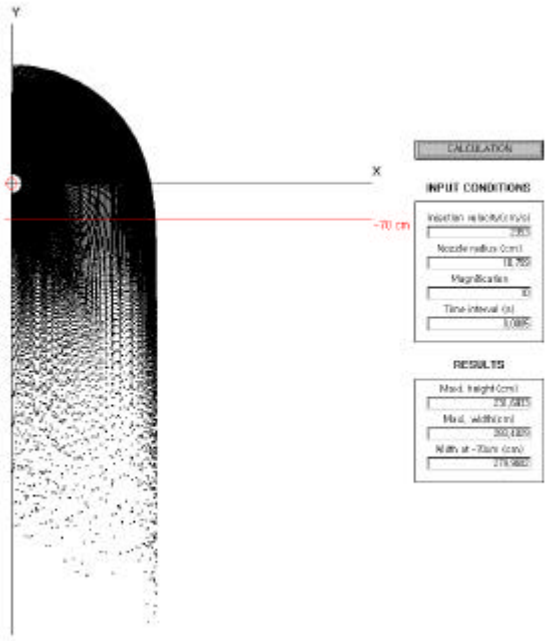

Fig. 11 Flow pattern under the same condition as in the DVI system

Table 5. Results of the computation with the DVI system

Injection Velocity	2353 cm/s
Height	231.69 cm
Half Width at –70 cm	279.96 cm
Half Width (Maximum)	283.40 cm

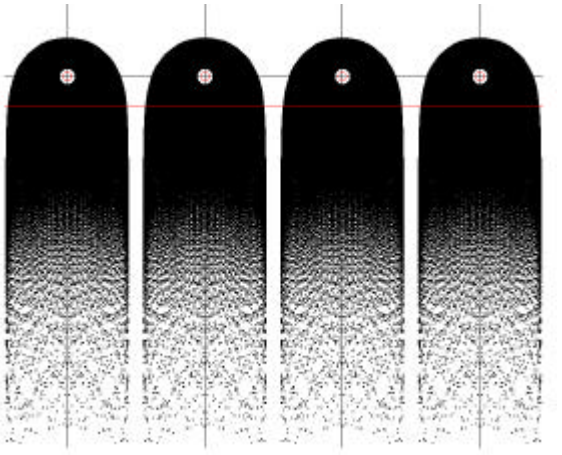

Fig. 12 Flow distribution at v = 500 cm/s

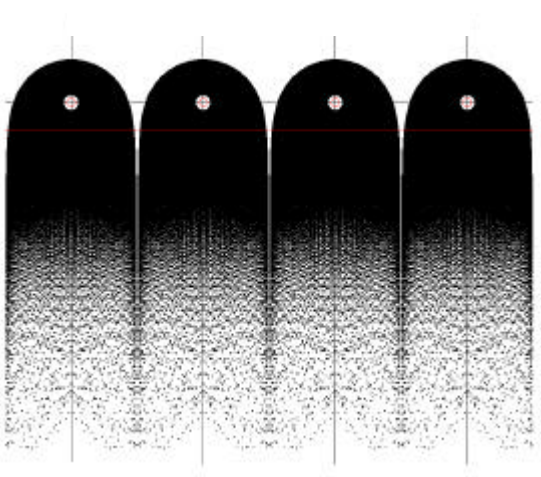

Fig. 13 Flow distribution at v = 600 cm/s

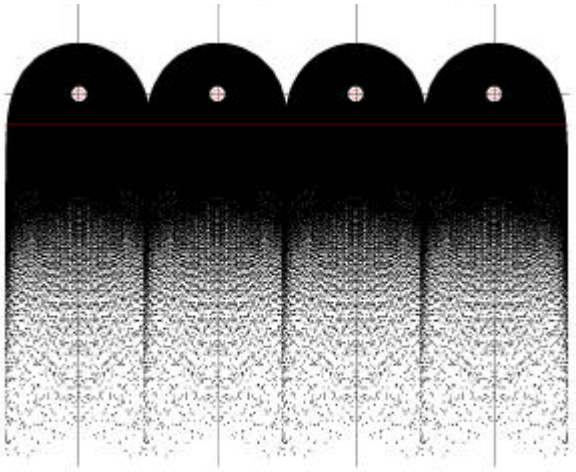

Fig. 14 Flow distribution at v = 700 cm/s

Figure 12 shows that the injection flows do not interfere with each other at v = 500 cm/s. As the injection velocity increases to 600 cm/s, the flows begin to get in touch at the bottom as shown in Fig.13. At v = 700 cm/s, the flow interference starts right from the injection points as shown in Fig.14.

5. CONCLUSION

Experiments were conducted using the flat acryl plates. The conductance method was used to measure the flow width along with visual inspection. It was found that the flow width increases downstream. The outer boundary of the fluid flow was thick. Also, the greater the injection velocity, the larger the flow width and the smaller the average film thickness. To understand the impingement flow characteristics observed from the tests, a simple numerical code was written to analyze the flow pattern. The program utilizes the potential function and the Navier-Stokes equations in the impingement region and the wall jet region, respectively. Except the experimental error of fluctuations on the plate, the predictions were in fair agreement with the measured data. In reactor applications, flows from the four DVI lines were predicted to get in touch with one another in the downcomer depending the injection flow velocity. Experimental and numerical results shed light on the width of the DVI flow, which is critical in determining the amount of ECC bypass due to flooding.

REFERENCES

Coleman, D. D. and Richard, S. S. (1971). “A study of free jet impingement. Part 1. Mean properties of free and impinging jets,” *J. Fluid Mech.* Vol 45, 281-319.

Mohan, D. D. and Ramesh, H. V. (1982). “Submerged laminar jet impingement on a plane”, *J. Fluid Mech.* Vol. 114, 213-235.

Safety Code Development Group, (1984). "TRAC-PF1: An Advanced Best-Estimate Computer Program for Pressurized Water Reactor Analysis," NUREG/CR-3567 LA-9944-MS, Los Alamos National Laboratory, Los Alamos, NM, U.S.A.

Suh, K. Y., et al., (1998). "Direct Vessel Injection Testing of Emergency Core Cooling Water," KAERI/CM-304/98, Korea Atomic Energy Research Institute, Taejon, Korea.

White, F.M. (1999), *Fluid Mechanics*, 4th Edition, McGraw-Hill Companies, Inc., Singapore.